micromachines

MDPI

Article

Growth of a Large, Single-Crystalline WS_2 Monolayer for High-Performance Photodetectors by Chemical Vapor Deposition

Ying Chen [1,2,3]

[1] Hubei Engineering Technology Research Center of Energy Photoelectric Device and System, Hubei University of Technology, Wuhan 430068, China; chenyddc@163.com
[2] Hubei Collaborative Innovation Center for High-Efficient Utilization of Solar Energy, Wuhan 430068, China
[3] School of Science, Hubei University of Technology, Wuhan 430068, China

Abstract: 2D WS_2 is a promising candidate for the next generation nanoelectronics, spintronics, valleytronics, and optoelectronics. However, the uncontrollably large-area growth of WS_2 nanosheets and their unsatisfactory performance of the photodetectors based on WS_2 hindered its applications. Here, we proposed a CVD method using tungstic acid as the precursors to grow WS_2 flakes. After being characterized by AFM, Raman, PL, and TEM, we found the as-grown WS_2 flakes were high-quality structures. Then the photodetectors based on the as-grown WS_2 were fabricated, which exhibited high responsivity (7.3 A W^{-1}), a fast response rate (a response time of 5 ms and a recovery time of 7 ms), prefect external quantum efficiency (EQE) (1814%), and remarkable detectivity (D^*) (3.4×10^{12} Jones). Our works provided a new CVD method to grow some high-quality WS_2 nanosheets.

Keywords: WS_2 flakes; tungstic acid; chemical vapor deposition; photodetectors

Citation: Chen, Y. Growth of a Large, Single-Crystalline WS_2 Monolayer for High-Performance Photodetectors by Chemical Vapor Deposition. *Micromachines* **2021**, *12*, 137. https://doi.org/10.3390/mi12020137

Academic Editor: Ha Duong Ngo
Received: 17 December 2020
Accepted: 25 January 2021
Published: 27 January 2021

1. Introduction

Atomically thin tungsten disulfide (WS_2), a 2D crystal with some interesting and important properties, is a promising candidate for the next generation of nanoelectronics, spintronics, valleytronics, and optoelectronics [1–7]. For example, WS_2 has a direct bandgap in the visible range and high absorption relative to its thickness [5,8]. WS_2 exhibits ambipolar field-modulation behavior [9]. The theoretical calculations predict that it has a reduced effective mass, allowing higher carrier mobility [10]. Monolayer WS_2 has strong PL emission efficiency, stronger than other TMDCs [11,12]. WS_2 exhibits strong spin-orbit coupling and band splitting due to spin enabling spintronics/valleytronics [13–16]. WS_2 also has high nonlinear susceptibility, suggesting its use for nonlinear optical devices [17,18]. Nevertheless, most researchers on WS_2 are largely limited because of the relatively small lateral size of exfoliated flakes, not to mention the randomness of their shape, thickness, and crystal quality [19,20]. Liquid exfoliation has an advantage for the mass production of WS_2, but it is difficult to control defects, hindering its application to electronic devices [21–23]. CVD is a hopeful approach to grow large-area WS_2 flakes for extensive device applications. There are two common methods to synthesize WS_2 by supplying tungsten sources on inert substrates before sulfurization in CVD. One is thin tungsten films or thin tungsten oxide films deposited by various methods including e-beam evaporation, magnetron sputtering, and atomic layer deposition [11,24–29]. The other is that of tungsten oxides solid precursors vaporized with solid sulfur sources simultaneously during the CVD process [30–34]. As it is difficult to control the tungsten sources location, distribution, and uniformity precisely, and the poor adhesion of the sources to inert substrates, the controlled CVD growth of large-area uniform monolayer WS_2 remains a challenge. Some groups used metal substrates (Au) instead of the inert substrates to synthesize a large-area monolayer WS_2 film; they also tested the electrical properties of WS_2-based field-effect transistors

after bubbling transfer from Au substrates to SiO_2/Si substrates [35–37]. Here we report a new method, spin-coating tungsten acid as a tungsten source on SiO_2/Si substrates directly before sulfurization, to grow single crystalline WS_2 monolayers with a size of up to hundreds of micrometers. We also found that photodetectors based on single crystalline WS_2 flakes have a high responsivity of 7.3 A W^{-1} with a fast response rate of 5 ms, an external quantum efficiency (*EQE*) of 1814%, and a detectivity (D^*) of 3.4 × 10^{12} Jones.

2. Materials and Methods

The WS_2 flakes were synthesized by using tungstic acid on SiO_2/Si substrates as the precursors and sulfurizing via a chemical vapor deposition (CVD) method. First, 2.8 g of tungstic acid (99.9%, Alfa) was dispersed in the oxalic acid solution (0.15 M/L) by ultrasound. Then the tungstic acid colloidal solution was dispersed on a clean SiO_2/Si substrate by spin-coating. After that, the whole substrate was annealed in air at 100 °C for 1h. Finally, the SiO_2/Si substrates with tungstic acid were sulfurized by CVD. For CVD growth, the Si/SiO_2 substrates with the tungstic acid colloidal solution were placed at the center of the quartz tube, and the 0.1 g S powders (99.5%, Alfa) were placed on the upstream side of the Si/SiO_2 substrates. The quartz tube was flushed with Ar (5N) gas several times and purged to 0.1 Pa with a mechanical pump. The furnace temperature was raised to 900 °C in 30 min and kept for 30 min with a flow rate of 50 sccm Ar gas. After growth, the furnace was naturally cooled to room temperature. The synthesized WS_2 samples were characterized by an atomic force microscope (AFM, SPM9700, Shimadzu), Raman spectroscopy, and a transmission electron microscope (TEM, Tecnai G^2 F30 S-TWIN, FEI). The Raman spectra were recorded in the backscattering geometry at a 532 nm line with an argon ion laser Raman spectrometer (LabRAM HR800, Horiba JobinYvon). The Raman mappings were collected by alpha300 R, WITec GmbH, Ulm, Germany, the laser wavelength was 532 nm, and the scanning step interval was 300 nm.

We fabricated the photodetectors based on the WS_2 flakes by a standard photolithography procedure (MDA-400M, Midas). The 10/50 nm Ti/Au electrode patterns were deposited by an E-beam deposition system (Nexdep, Angstrom Engineering). The photodetector measurement devices contained a broadband laser-driver light source (LDLS, EQ-1500, Energetiq) calibrated by a UV-enhanced silicon photodiode in an ambient atmosphere, a semiconductor characterization system (4200-SCS, Keithley), and an oscilloscope (DSO-X 3052A, Keysight). The oscilloscope light pulse chopped was 500 nm, and the frequency was 3 Hz.

3. Results and Discussion

Figure 1a shows the optical image of the as-grown triangle WS_2 flakes on SiO_2/Si substrate; the majority of the flakes were more than 220 μm. The thickness of these triangle crystals was measured by atomic force microscopy (AFM) (Figure 1b). The AFM step height of the WS_2 flake was typically measured at 0.7 nm, which corresponds to a one-layer structure.

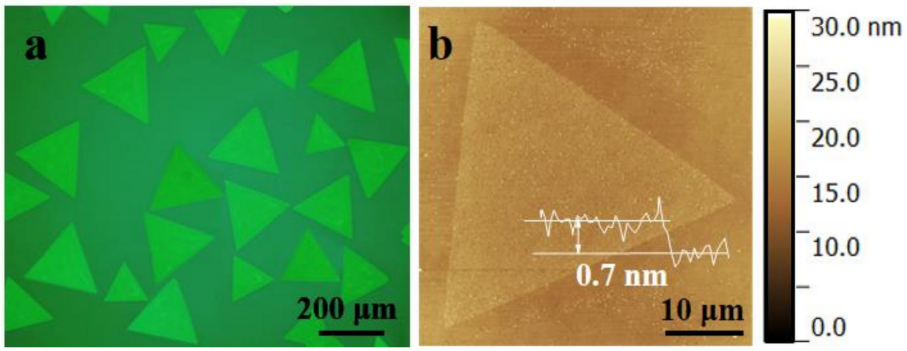

Figure 1. (**a**) Optical microscope images of the monolayer WS_2. (**b**) AFM images of the monolayer WS_2.

We have further investigated the layer number of the resulting atomically thin WS_2 triangles by Raman spectroscopy. As shown in Figure 2a, the strongest peak of the WS_2 triangle flake at about 350 cm^{-1} includes three subpeaks, which are resolved by a multipeak Lorentzian fitting. According to the calculated phonon dispersion [38] and experimental studies [13,39–41] of 1L-WS_2, the in-plane vibrational E^1_{2g}(M) mode peak is at 343 cm^{-1}, the second-order mode of longitudinal acoustic phonon 2LA (M) peak is at 350 cm^{-1}, and the in-plane vibrational E^1_{2g}(Γ) mode peak is at 355 cm^{-1}, respectively. The other peaks at 418, 295, and 322 cm^{-1} are attributed to the out-of-plane A_{1g}(Γ) mode, the combination modes of 2LA(M)-2E^2_{2g}(Γ), and the combination modes of 2LA(M)-E^2_{2g}(Γ), respectively. The spectral fingerprint of a monolayer WS_2 is the frequency separation of 62 cm^{-1} between the E^1_{2g}(Γ) mode and the A_{1g}(Γ) mode [11]. Raman images (Figure 2b,c) plotted by extracting the intensity were acquired to demonstrate the uniformity of our WS_2 samples. The 2LA(M) phonon mode was much more intense than the A_{1g}(Γ) mode. The as-grown WS_2 triangle flake was uniform.

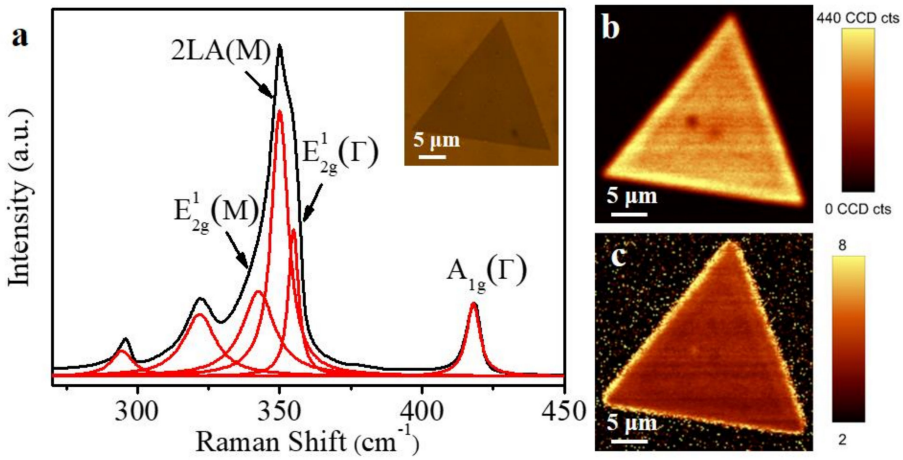

Figure 2. (**a**) Raman characterization of the monolayer WS_2 triangle flake with 532 nm excitation wavelengths. (**b**) A1g(Γ) intensity mapping for the WS_2 triangle flake. (**c**) Intensity ratio mapping of 2LA(M) over A1g(Γ) for the WS_2 triangle flake.

The optical properties of the monolayer WS_2 triangle flakes were further investigated by microphotoluminescence (PL). The monolayer WS_2 flake has a PL peak at about 642 nm, and its full width half maximum (FWHM) value is 22 nm (Figure 3a). The corresponding PL peak-integrated intensity, position, and width mappings of the monolayer WS_2 triangle flake are shown in Figure 3b–d, respectively. The results of the PL indicated the as-grown WS_2 was defect free and uniform.

The structures of the monolayer WS_2 triangle flakes were characterized by TEM. Figure 4a shows the low magnitude bright-field TEM image of a WS_2 triangular crystal. The high-resolution TEM (HRTEM) image (Figure 4b) shows the hexagonal lattice fringes, which indicates a perfect atomic structure with a lattice spacing of 0.27 nm, corresponding to the (100) planes. The corresponding selected area electron diffraction (SAED) pattern (Figure 4c) revealed the defect free nature of the WS_2 flake [36]. Then the elemental compositions of the WS_2 triangle flakes were acquired by EDX mapping and EDX spectrum. EDX mapping in Figure 4d,e indicates the W and S elements distribute evenly. EDX spectrum in Figure 4f demonstrates the atomic ratio of W and S is around 1:2, which is consistent with the original stoichiometry of WS_2. The TEM results further prove that as-grown WS_2 flakes are defect free.

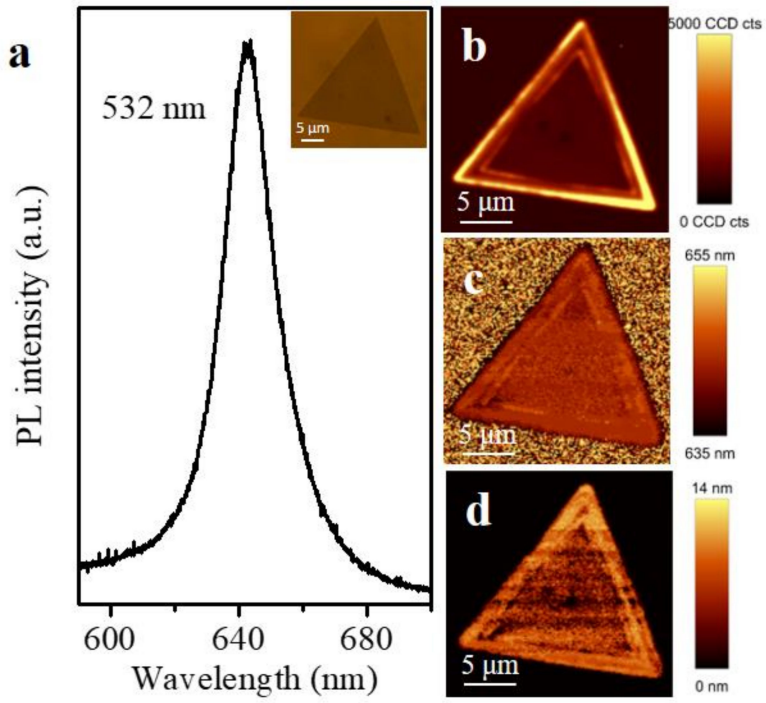

Figure 3. (**a**) PL spectra of the monolayer WS_2 triangle flake. (**b**–**d**) PL images of the peak integrated intensity, position, and width, respectively.

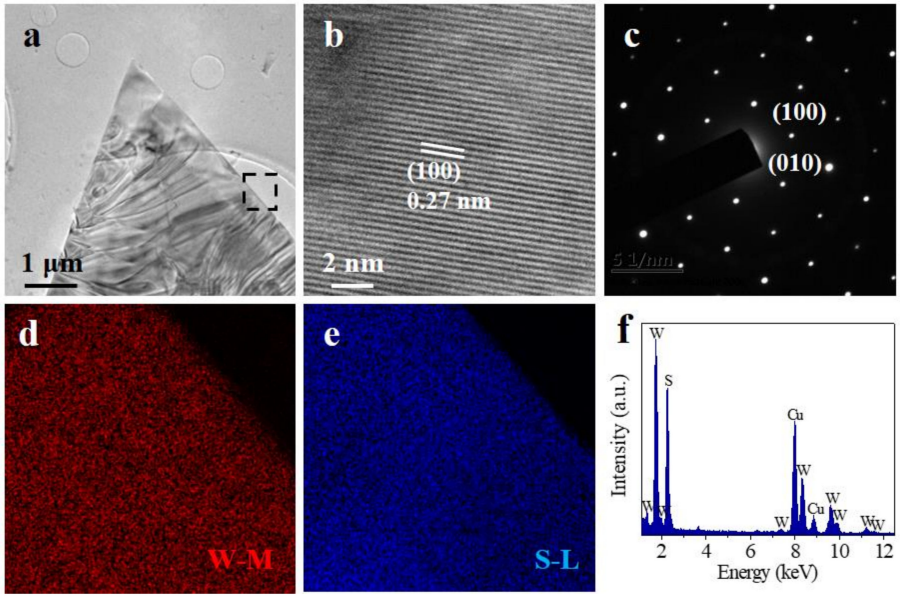

Figure 4. (**a**) Low-magnification TEM image of the WS_2 triangle flake. (**b**) High-resolution TEM image and (**c**) SAED pattern image of the WS_2 triangle flake. (**d**,**e**) W and S elemental mapping in the black rectangle region of the WS_2 flake in (**a**,**f**) EDX spectrum of the WS_2 flake.

To research the optoelectronic properties of the WS_2 flakes, photodetectors based on them were fabricated. The spectral response curve reaches a minimum at the wavelength of ≈645 nm in Figure 5a. Hence, the bandgap is about 1.92 eV by calculation, which is consistent with the PL results. Fitting the plot of photocurrent I_{ph} on light intensity P for the WS_2 flake as $I_{ph} \approx P^{\theta}$ obtains the value of $\theta \approx 0.96$ (Figure 5b), hinting the as-grown WS_2 has very few defects or traps to photo-induced electron/hole pairs in the test power density range [42]. We further tested the cyclability of the photodetector under 500 nm incident light with the light on/off time interval of 30 s under a bias of 1 V (Figure 5c).

The performances of the photodetector are stable. The response and recovery rates were 5 ms and 7 ms tested by an oscilloscope, respectively (Figure 5d). The photoresponsivity was 7.3 A W^{-1}, according to the $R_\lambda = I_{ph}/PS$, where I_{ph} is the photoexcited current, P is the light power intensity, and S is the effective area of the photodetector. The external quantum efficiency (EQE) was 1814%, according to the EQE = $hcR_\lambda/e\lambda$, where h is the Plank's constant, c is the light velocity, R_λ is the photoresponsivity, e is the elementary electronic charge, and λ is the exciting wavelength. The specific detectivity (D^*) was 3.4×10^{12} Jones, according to the $D^* = R_\lambda S^{1/2}/(2eI_{dark})^{1/2}$, where I_{dark} is the dark current. The performance of our photodetector is more inspiring than the most reported WS_2 based photodetectors shown in Table 1.

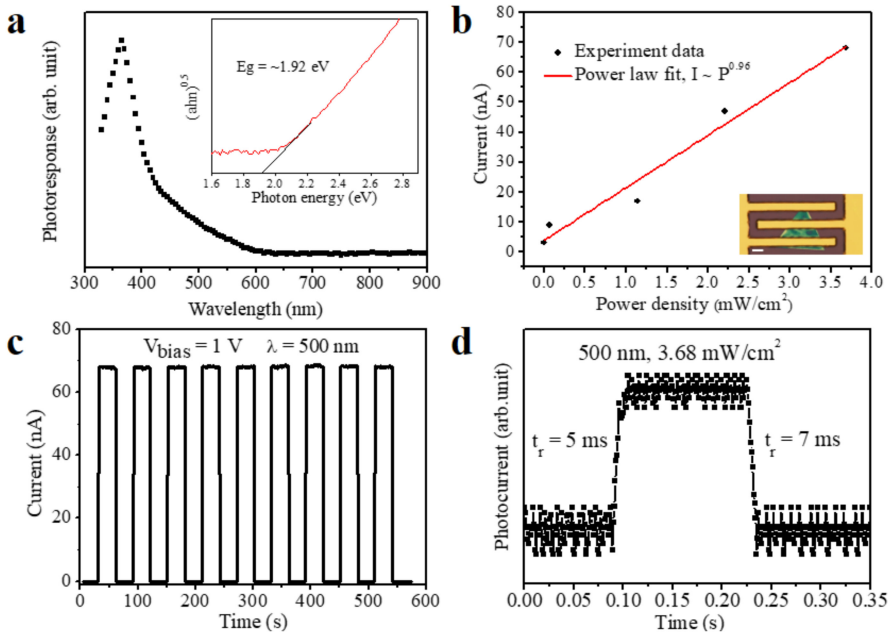

Figure 5. Optoelectronic properties of the WS_2 triangle flake. (**a**) The spectral response curve of the WS_2 triangle flake. Inset: the fitting curve of obtaining the bandgap. (**b**) Photocurrent as a function of illumination intensity at V_{bias} = 1 V. Inset: the optical image of the WS_2 photodetector; the scale bar is 10 μm. (**c**) Time-resolved photoresponse of the WS_2 photodetector under a bias voltage of 1 V and illumination power of 3.68 mW·cm^{-2}. (**d**) Response and recovery curves.

Table 1. Comparison of the key parameters of our photodetector.

Photodetectors	Fabrication Method	R_λ (A/W)	EQE (%)	Response Time (ms)	Reference
Multilayer WS_2	CVD	92×10^{-6}	-	5.3	[4]
Multilayer WS_2	Exfoliated	5.7	1118	<20	[43]
Monolayer WS_2	CVD	18.8×10^{-3}	-	<4.5	[44]
Multilayer WS_2	PLD	0.51	137	4.1×10^{-3}	[45]
Monolayer WS_2	CVD	3.07	763	370	[46]
Multilayer WS_2	Drop casting	145×10^{-3}	-	153.78	[47]
Monolayer WS_2	CVD	7.3	1814	5	This work

4. Conclusions

In summary, we grew the monolayer WS_2 triangle flakes via a CVD method with the tungstic acid, and researched the performance of the photodetectors based on them. The utilization of tungstic acid colloidal solution could improve the uniformity of the tungsten sources on the substrates. The as-grown monolayer WS_2 flakes have a size of about 220 μm, a bandgap of about 1.92 eV, and no defects. The photodetectors based on them showed

excellent performance, such as high responsivity of 7.3 A W^{-1}, large EQE of 1814%, and a fast response rate of 5 ms.

Funding: This research was funded by the Natural Science Foundation of China, grant number 21701041; the Open Foundation of Hubei Collaborative Innovation Center for High-efficiency Utilization of Solar Energy, grant number HBSKFQN2017001; and the Talents of high-level scientific research foundation of the Hubei University of Technology, grant number BSQD2017010.

Institutional Review Board Statement: Not applicable.

Informed Consent Statement: Not applicable.

Data Availability Statement: No new data were created or analyzed in this study. Data sharing is not applicable to this article.

Conflicts of Interest: The authors declare no conflict of interest.

References

1. Manzeli, S.; Ovchinnikov, D.; Pasquier, D.; Yazyev, O.V.; Kis, A. 2D transition metal dichalcogenides. *Nat. Rev. Mater.* **2017**, *2*, 17033. [CrossRef]
2. Schmidt, H.; Giustiniano, F.; Eda, G. Electronic transport properties of transition metal dichalcogenide field-effect devices: Surface and interface effects. *Chem. Soc. Rev.* **2015**, *44*, 7715–7736. [CrossRef] [PubMed]
3. Chhowalla, M.; Liu, Z.F.; Zhang, H. Two-dimensional transition metal dichalcogenide (TMD) nanosheets. *Chem. Soc. Rev.* **2015**, *44*, 2584–2586. [CrossRef] [PubMed]
4. Perea-López, N.; Elías, A.L.; Berkdemir, A.; Castro-Beltran, A.; Gutiérrez, H.R.; Feng, S.; Lv, R.; Hayashi, T.; López-Urías, F.; Ghosh, S.; et al. Photosensor device based on few-layered WS_2 films. *Adv. Funct. Mater.* **2013**, *23*, 5511–5517. [CrossRef]
5. Eda, G.; Maier, S.A. Two-dimensional crystals: Managing light for optoelectronics. *ACS Nano* **2013**, *7*, 5660–5665. [CrossRef]
6. Jeong, H.Y.; Jin, Y.; Yun, S.J.; Zhao, J.; Baik, J.; Keum, D.H.; Lee, H.S.; Lee, Y.H. Heterogeneous defect domains in single-crystalline hexagonal WS_2. *Adv. Mater.* **2017**, *29*, 1605043. [CrossRef]
7. Lan, C.Y.; Zhou, Z.Y.; Zhou, Z.F.; Li, C.; Shu, L.; Shen, L.F.; Li, D.P.; Dong, R.T.; Yin, S.P.; Ho, J.C. Wafer-scale synthesis of monolayer WS_2 for high-performance flexible photodetectors by enhanced chemical vapor deposition. *Nano Res.* **2018**, *11*, 3371–3384. [CrossRef]
8. Zhou, B.; Yang, L.X.; Chen, F.; Xu, M.; Wu, T.; Wu, G.; Chen, X.H.; Feng, D.L. Evolution of electronic structure in $Eu_{1-x}La_xFe_2As_2$. *J. Phys. Chem. Solids* **2011**, *72*, 474478. [CrossRef]
9. Sik Hwang, W.; Remskar, M.; Yan, R.; Protasenko, V.; Tahy, K.; Doo Chae, S.; Zhao, P.; Konar, A.; Xing, H.; Seabaugh, A.; et al. Transistors with chemically synthesized layered semiconductor WS_2 exhibiting 105 room temperature modulation and ambipolar behavior. *Appl. Phys. Lett.* **2012**, *101*, 13107. [CrossRef]
10. Liu, L.; Kumar, S.B.; Ouyang, Y.; Guo, J. Performance limits of monolayer transition metal dichalcogenide transistors. *IEEE Trans. Electron Dev.* **2011**, *58*, 3042–3047. [CrossRef]
11. Gutierrez, H.R. Extraordinary room-temperature photoluminescence in triangular WS_2 monolayers. *Nano Lett.* **2013**, *13*, 3447–3454. [CrossRef] [PubMed]
12. Zhao, W.J. Evolution of electronic structure in atomically thin sheets of WS_2 and WSe_2. *ACS Nano* **2013**, *7*, 791–797. [CrossRef] [PubMed]
13. Zeng, H.; Liu, G.B.; Dai, J.; Yan, Y.; Zhu, B.; He, R.; Xie, L.; Xu, S.; Chen, X.; Yao, W.; et al. Optical signature of symmetry variations and spin-valley coupling in atomically thin tungsten dichalcogenides. *Sci. Rep.* **2013**, *3*, 1608. [CrossRef]
14. Xiao, D.; Liu, G.B.; Feng, W.; Xu, X.; Yao, W. Coupled spin and valley physics in monolayers of MoS_2 and other group-VI dichalcogenides. *Phys. Rev. Lett.* **2012**, *108*, 196802. [CrossRef] [PubMed]
15. Cao, T.; Wang, G.; Han, W.; Ye, H.; Zhu, C.; Shi, J.; Niu, Q.; Tan, P.; Wang, E.; Liu, B.; et al. Valley-selective circular dichroism of monolayer molybdenum disulphide. *Nat. Commun.* **2012**, *3*, 887. [CrossRef]
16. Zhu, Z.Y.; Cheng, Y.C.; Schwingenschlögl, U. Giant spin-orbit-induced spin splitting in two-dimensional transition-metal dichalcogenide semiconductors. *Phys. Rev. B* **2011**, *84*, 153402. [CrossRef]
17. Janisch, C.; Mehta, N.; Ma, D.; Elías, A.L.; Perea-López, N.; Terrones, M.; Liu, Z. Ultrashort optical pulse characterization using WS_2 monolayers. *Opt. Lett.* **2014**, *39*, 383–385. [CrossRef]
18. Janisch, C.; Wang, Y.; Ma, D.; Mehta, N.; Elías, A.L.; Perea-López, N.; Terrones, M.; Crespi, V.; Liu, Z. Extraordinary second harmonic generation in tungsten disulfide monolayers. *Sci. Rep.* **2014**, *4*, 5530. [CrossRef]
19. Georgiou, T.; Yang, H.; Jalil, R.; Chapman, J.; Novoselov, K.S.; Mishchenko, A. Electrical and optical characterization of atomically thin WS_2. *Dalton Trans.* **2014**, *43*, 10388–10391. [CrossRef]
20. Ovchinnikov, D.; Allain, A.; Huang, Y.S.; Dumcenco, D.; Kis, A. Electrical transport properties of single-layer WS_2. *ACS Nano* **2014**, *8*, 8174–8181. [CrossRef]
21. Chhowalla, M. The chemistry of two-dimensional layered transition metal dichalcogenide nanosheets. *Nature Chem.* **2013**, *5*, 263–275. [CrossRef] [PubMed]

22. Coleman, J.N.; Lotya, M.; O'Neill, A.; Bergin, S.D.; King, P.J.; Khan, U.; Young, K.; Gaucher, A.; De, S.; Smith, R.J.; et al. Two-dimensional nanosheets produced by liquid exfoliation of layered materials. *Science* **2011**, *331*, 568–571. [CrossRef] [PubMed]
23. Nicolosi, V.; Chhowalla, M.; Kanatzidis, M.G.; Strano, M.S.; Coleman, J.N. Liquid exfoliation of layered materials. *Science* **2013**, *340*, 1226419. [CrossRef]
24. Song, J.G.; Park, J.; Lee, W.; Choi, T.; Jung, H.; Lee, C.W.; Hwang, S.H.; Myoung, J.M.; Jung, J.H.; Kim, S.H.; et al. Layer-controlled, wafer-scale, and conformal synthesis of tungsten disulfide nanosheets using atomic layer deposition. *ACS Nano* **2013**, *7*, 11333–11340. [CrossRef] [PubMed]
25. Orofeo, C.M.; Suzuki, S.; Sekine, Y.; Hibino, H. Scalable synthesis of layer-controlled WS_2 and MoS_2 sheets by sulfurization of thin metal films. *Appl. Phys. Lett.* **2014**, *105*, 83112. [CrossRef]
26. Elías, A.L.; Perea-López, N.; Castro-Beltrán, A.; Berkdemir, A.; Lv, R.; Feng, S.; Long, A.D.; Hayashi, T.; Kim, Y.A.; Endo, M.; et al. Controlled synthesis and transfer of large-area WS_2 Sheets: From single layer to few layers. *ACS Nano* **2013**, *7*, 5235–5242. [CrossRef]
27. Jung, Y.; Shen, J.; Liu, Y.; Woods, J.M.; Sun, Y.; Cha, J.J. Metal seed layer thickness-induced transition from vertical to horizontal growth of MoS_2 and WS_2. *Nano Lett.* **2014**, *14*, 6842–6849. [CrossRef]
28. Morrish, R.; Haak, T.; Wolden, C.A. Low-Temperature Synthesis of n-type WS_2 thin films via H_2S plasma sulfurization of WO_3. *Chem. Mater.* **2014**, *26*, 3986–3992. [CrossRef]
29. Zhou, S.; Liu, L.; Cui, S.; Ping, X.; Hu, D.; Jiao, L. Fast growth of large single-crystalline WS_2 monolayers via chemical vapor deposition. *Nano Res.* **2020**. [CrossRef]
30. Fu, Q.; Wang, W.; Yang, L.; Huang, J.; Zhang, J.; Xiang, B. Controllable synthesis of high quality monolayer WS_2 on a SiO_2/Si substrate by chemical vapor deposition. *RSC Adv.* **2015**, *5*, 15795–15799. [CrossRef]
31. Zhang, Y.; Zhang, Y.; Ji, Q.; Ju, J.; Yuan, H.; Shi, J.; Gao, T.; Ma, D.; Liu, M.; Chen, Y.; et al. Controlled growth of high-quality monolayer WS_2 layers on sapphire and imaging its grain boundary. *ACS Nano* **2013**, *7*, 8963–8971. [CrossRef] [PubMed]
32. Cong, C.; Shang, J.; Wu, X.; Cao, B.; Peimyoo, N.; Qiu, C.; Sun, L.; Yu, T. Synthesis and optical properties of large-area single-crystalline 2D semiconductor WS_2 monolayer from chemical vapor deposition. *Adv. Opt. Mater.* **2014**, *2*, 131–136. [CrossRef]
33. Okada, M.; Sawazaki, T.; Watanabe, K.; Taniguch, T.; Hibino, H.; Shinohara, H.; Kitaura, R. Direct chemical vapor deposition growth of WS_2 atomic layers on hexagonal boron nitride. *ACS Nano* **2014**, *8*, 8273–8277. [CrossRef] [PubMed]
34. Han, J.; Fang, R.; Zhu, L.; Geng, Z.; He, X. CVD growth of monolayer WS_2 through controlled growth temperature and time. *Ferroelectrics* **2020**, *562*, 51–57. [CrossRef]
35. Yun, S.J.; Chae, S.H.; Kim, H.; Park, J.C.; Park, J.H.; Han, G.H.; Lee, J.S.; Kim, S.M.; Oh, H.M.; Seok, J.; et al. Synthesis of centimeter-scale monolayer tungsten disulfide film on gold foils. *ACS Nano* **2015**, *9*, 5510–5519. [CrossRef]
36. Gao, Y.; Liu, Z.; Sun, D.M.; Huang, L.; Ma, L.P.; Yin, L.C.; Ma, T.; Zhang, Z.; Ma, X.L.; Peng, L.M.; et al. Large-area synthesis of high-quality and uniform monolayer WS_2 on reusable Au foils. *Nat. Commun.* **2015**, *6*, 8569. [CrossRef] [PubMed]
37. Zhang, Y.; Shi, J.; Han, G.; Li, M.; Ji, Q.; Ma, D.; Zhang, Y.; Li, C.; Lang, X.; Zhang, Y.; et al. Chemical vapor deposition of monolayer WS_2 nanosheets on Au foils toward direct application in hydrogen evolution. *Nano Res.* **2015**, *8*, 2881–2890. [CrossRef]
38. Molina-Sánchez, A.; Wirtz, L. Phonons in single-layer and few-layer MoS_2 and WS_2. *Phys. Rev. B* **2011**, *84*, 155413. [CrossRef]
39. Lee, Y.H.; Yu, L.; Wang, H.; Fang, W.; Ling, X.; Shi, Y.; Lin, C.T.; Huang, J.K.; Chang, M.T.; Chang, C.S.; et al. Synthesis and transfer of single-layer transition metal disulfides on diverse surfaces. *Nano Lett.* **2013**, *13*, 1852–1857. [CrossRef]
40. Berkdemir, A.; Gutierrez, H.R.; Botello-Mendez, A.R.; Perea-Lopez, N.; Elias, A.L.; Chia, C.I.; Wang, B.; Crespi, V.H.; Lopez-Urias, F.; Charlier, J.C.; et al. Identification of individual and few layers of WS_2 using Raman Spectroscopy. *Sci. Rep.* **2013**, *3*, 1755. [CrossRef]
41. Zhao, W.; Ghorannevis, Z.; Amara, K.K.; Pang, J.R.; Toh, M.; Zhang, X.; Kloc, C.; Tan, P.H.; Eda, G. Lattice dynamics in mono- and few-layer sheets of WS_2 and WSe_2. *Nanoscale* **2013**, *5*, 9677–9683. [CrossRef] [PubMed]
42. Kind, H.; Yan, H.Q.; Messer, B.; Law, M.; Yang, P.D. Nanowire ultraviolet photodetectors and optical switches. *Adv. Mater.* **2002**, *14*, 158–160. [CrossRef]
43. Huo, N.J.; Yang, S.X.; Wei, Z.M.; Li, S.S.; Xia, J.B.; Li, J.B. Photoresponsive and gas sensing field-effect transistors based on multilayer WS_2 nanoflakes. *Sci. Rep.* **2014**, *4*, 5209. [CrossRef] [PubMed]
44. Lan, C.Y.; Li, C.; Yin, Y.; Liu, Y. Large-area synthesis of monolayer WS_2 and its ambient-sensitive photo-detecting performance. *Nanoscale* **2015**, *7*, 5974–5980. [CrossRef] [PubMed]
45. Yao, J.D.; Zheng, Z.Q.; Shao, J.M.; Yang, G.W. Stable, highly-responsive and broadband photodetection based on large-area multilayered WS_2 films grown by pulsed-laser deposition. *Nanoscale* **2015**, *7*, 14974–14981. [CrossRef]
46. Chen, Y.; Gan, L.; Li, H.; Ma, Y.; Zhai, T.Y. Achieving uniform monolayer transition metal dichalcogenides film on silicon wafer via silanization treatment: A typical study on WS_2. *Adv. Mater.* **2017**, *29*, 1603550. [CrossRef]
47. Harith, A.; Haroon, R. 405 nm ultraviolet photodetector based on tungsten disulphide thin film grown by drop casting method. *J. Mod. Optic.* **2019**, *66*, 1836–1840. [CrossRef]